

Detailed quantum-chromodynamic predictions for high- p_T processes

J. F. Owens and E. Reya*

Department of Physics, Florida State University, Tallahassee, Florida 32306

M. Glück

Institut für Physik, Universität Mainz, 6500 Mainz, West Germany

(Received 12 January 1978)

High- p_T single-particle inclusive cross section calculations are presented for the CERN ISR and ISABELLE energy ranges, taking into account *all* lowest-order hard-scattering subprocesses required by quantum chromodynamics (QCD). The input quark and gluon distribution and fragmentation functions were determined from analyses of deep-inelastic lepton data and were subject to various theoretical constraints such as sum rules and SU(3) symmetry. We thoroughly discuss the effects of the individual contributions from fermionic and gluonic subprocesses, as well as those effects stemming from QCD scaling violations in parton distributions and/or fragmentation functions. In particular, the inclusion of the large elastic gluon-gluon and gluon-quark scattering terms has a profound effect on both the normalization and the p_T dependence of the predictions. The p_T and θ dependences of single- π^0 production are shown to be in good agreement with available data in the region $p_T \gtrsim 4.5$ GeV/ c and $\sqrt{s} \gtrsim 50$ GeV. In addition, we predict and discuss various ratios for inclusive single-particle production of π^+ , π^- , K^+ , and K^- , which also turn out to be in excellent agreement with presently available experiments.

I. INTRODUCTION

The success of the parton model in describing the lepton-induced processes in the deep-inelastic region has led to the application¹ of this model to the study of hadron-induced reactions in the large- p_T region, where the short-distance part of the strong interactions is expected to dominate. In this most naive scale-invariant version of the hard-collision model,^{1,2} where a *single hard* collision between the constituents (quarks) of the incident hadrons is responsible for the observed high- p_T secondaries, one expects the invariant inclusive single-particle cross section to decrease as p_T^{-4} at fixed center-of-mass scattering angle θ and fixed $x_T = 2p_T/\sqrt{s}$. However, at currently attainable energies the experimental data seem to scale roughly as p_T^{-8} for $p_T \lesssim 6$ GeV/ c . In order to rescue the naive hard-scattering model, one may take the empirical point of view that the high- p_T data are described by nonelementary subprocesses such as elastic quark-meson scattering (as in the constituent-interchange model³) without explaining the absence of elastic quark-quark scattering. Alternatively one may assume the presence of an unknown dynamical mechanism in order to account for the p_T^{-8} falloff.⁴ This latter purely phenomenological approach, exemplified by the work of Field and Feynman,⁴ lacks a theoretical explanation for the p_T^{-8} variation of the quark-quark cross section, and plausibility arguments using soft multigluon exchanges appear difficult to justify within the philosophy of *hard-collision* models. In either of these two options, one gives up predicting the p_T dependence by either fitting⁴ the p_T dependence of

the elementary subprocesses, or by postulating³ the dominance of quark-hadron subprocesses ($\sim p_T^{-8}$) without explaining the absence of quark-quark, gluon-quark, and gluon-gluon scattering ($\sim p_T^{-4}$).

The experimental observation that exact Bjorken scaling is violated in deep-inelastic electron-nucleon scattering has taught us that, at currently available energy resolutions, the constituents of hadrons are not pointlike. These features are naturally expected, and in fact have been anticipated, in any field theory of strong interactions, and can be successfully explained⁵⁻⁹ by asymptotically free gauge theories—the quantum chromodynamics (QCD) of the strong interactions. Thus, a gauge theory of colored quarks and gluons is widely considered to be the most promising candidate for the true theory of strong interactions. This point of view receives additional support from the fact that there are purely theoretical¹⁰ as well as phenomenological¹¹ indications against conventional, asymptotically nonfree field theories as serious candidates for describing strong interactions. Although short-distance arguments supplemented by renormalization-group techniques allow rather solid predictions for processes such as deep-inelastic lepton-nucleon scattering and e^+e^- annihilation, such methods are not immediately applicable to purely hadronic processes at large p_T , since these are not dominated by light-cone singularities in a straightforward way. Nevertheless, perturbation theory is still believed to be applicable to hard-collision models because of the fact that QCD is asymptotically free, which implies a small “strong” coupling constant $\alpha_s(Q^2)$ for large momen-

tum transfers, the only region of interest here. Despite some uncertainties in how to incorporate and calculate scaling violations in parton distributions as well as fragmentation functions, high- p_T processes may still provide important tests of QCD.

It has already been shown by Cahalan, Geer, Kogut, and Susskind¹² that lowest-order QCD quark-quark scattering, combined with scaling violations in parton distributions as calculated for deep-inelastic processes, cannot account for the high- p_T data, giving contributions which are about two orders of magnitude below the experiments and yielding p_T distributions which are still too flat. Subsequent analyses,¹³⁻¹⁵ still keeping only elastic quark-quark scattering as the relevant hard-collision subprocesses, have reached essentially the same conclusions unless one allows^{13, 14} for an unusually large, and theoretically unjustified, quark-gluon coupling constant α_{eff} . Taking into account the correct color factor $\frac{2}{9}$, typical values for α_{eff} are in the range of 2-4 which is about one order of magnitude larger than the QCD coupling α_s . Having arbitrarily fixed the absolute normalization in this way, one can account for the p_T^{-8} behavior of the invariant cross section by including¹³⁻¹⁵ the effects of scale breaking in the quark distributions and quark fragmentation functions. These scaling violations, obtained by fitting phenomenological parametrizations for the x and Q^2 dependence of structure functions to the deep-inelastic lepton-nucleon data at moderate values of Q^2 , have then to be extrapolated to the region of currently measured high- p_T data, typically to $Q^2 \approx 50-200 \text{ GeV}^2$. Some of these parametrizations¹⁴ represent the logarithmic QCD predictions for scaling deviations rather well, except for overestimating the Q^2 dependence in the threshold region, i.e., for x or z close to one, the region most sensitive to the fragmentation functions for currently available high- p_T data. Here, x denotes the fractional longitudinal momentum of a parton in a hadron, and z is the fractional momentum of a hadron coming from a parton. However, the scaling violations used in Refs. 13 and 15 are powerlike rather than logarithmic in Q^2 , which is not only in disagreement with QCD but might also strongly overestimate the importance of scale-breaking effects in high- p_T hadron processes.

If QCD and perturbation theory are indeed considered to be the theoretical basis for large- p_T hadron production, then it is certainly not sufficient to consider only elastic quark-quark scattering ($qq \rightarrow qq$) as the dominant subprocess, which constitutes at most a lower bound for the total production cross section. In addition to quarks, hadrons are presumed to contain colored vector gluons which can scatter off quarks and other gluons in an

approximately scale-invariant manner. From neutrino experiments we know¹⁶ that about 50% of the nucleon momentum is carried by this flavor neutral component—the gluons—the immediate importance of which is well known for explaining the scaling deviations in deep-inelastic reactions.^{5, 6, 8, 9} Although the detailed shape of the gluon distribution in the nucleon is not well known, dynamical QCD calculations^{5, 17} of parton distributions indicate that that of the gluon is sizable and non-negligible in the region relevant for present high- p_T experiments (typically $x \approx 0.2$). The gluon contribution can be even more pronounced if a naive counting-rule-like (flatter) distribution¹⁸ is considered. Thus, gluonic subprocesses such as $gq \rightarrow gq$, $gg \rightarrow q\bar{q}$, $q\bar{q} \rightarrow gg$, and $gg \rightarrow gg$ cannot be neglected *a priori* as compared to purely fermionic processes such as $qq \rightarrow qq$ and $q\bar{q} \rightarrow q\bar{q}$. The relevance of the $gg \rightarrow q\bar{q}$ subprocess has already been demonstrated for hadronic J/ψ production.¹⁹

Recently, attempts have been made to study gluonic contributions to high- p_T hadron production.^{20, 21} The results obtained in Ref. 20 show that, within the hard-scattering model, gluonic subprocesses as dictated by QCD are essential in explaining not only the absolute normalization of inclusive single-pion invariant cross sections at 90° , but also their correct p_T shape. Here we attempt a thorough analysis of single-particle inclusive data at various energies and angles for pions as well as kaons. These predictions as well as the ones for particle production charge ratios and x_T dependences are based on the full content of QCD. Contrary to the phenomenological approach advocated in Ref. 4, there are no free parameters left, once the various parton distributions and fragmentation functions are fixed by deep-inelastic lepton-nucleon data. Furthermore, we shall give simple parametrizations for pionic as well as kaonic parton fragmentation functions which satisfy theoretical sum rules and SU(3) symmetry (breaking) constraints, and compare them with recent semi-inclusive lepton data. In addition, we also study the effects of scaling violations in parton distributions as well as in fragmentation functions under the assumption, of course, that these are the same as predicted by QCD for deep-inelastic lepton-nucleon processes.

In Sec. II we present the basic expressions for the invariant cross section and discuss the various quark and gluon distributions used for our calculations; the quark and gluon decay functions are constrained to satisfy momentum and isospin sum rules, and we compare their predictions with recent semi-inclusive lepton data. We then proceed, in Sec. III, to predict the production of high- p_T π 's at CERN ISR and ISABELLE energies and at a

center-of-mass scattering angle $\theta = 90^\circ$, and to thoroughly discuss the effects of the individual contributions from fermionic and gluonic subprocesses to the total cross section. Furthermore, we compare our QCD predictions for the angular dependence of the invariant cross section with currently available data and give predictions for the x_T dependence at various energies and scattering angles. In addition, particle ratios of produced π^+ and K^+ are predicted and compared with the data. Our conclusions are summarized in Sec. IV and, for the sake of completeness, some details of the

elastic gluon-gluon cross-section calculation are given in the Appendix where we also summarize the expressions for the cross sections of the remaining relevant subprocesses.

II. GENERAL THEORETICAL FRAMEWORK

The invariant inclusive cross section for the reaction $A + B \rightarrow C + X$ for producing a hadron C at large p_T in the c.m. of A and B is given by (neglecting transverse momenta)^{1,2}

$$E_C \frac{d^3\sigma}{dp_C^3} = \frac{1}{\pi} \sum_{a,b,c,d} \int_{x_a^{\min}}^1 dx_a \int_{x_b^{\min}}^1 dx_b P_{a/A}(x_a, Q^2) P_{b/B}(x_b, Q^2) \frac{d\sigma^{ab \rightarrow cd}}{d\hat{t}} \frac{1}{z_C} D_{C/c}(z_C, Q^2), \quad (1)$$

where the sum over partons (a, b, c, d) includes gluons as well as quarks, and the longitudinal fractions $x_a = p_a/p_A$, $x_b = p_b/p_B$, and $z = z_C = p_C/p_C$ determine the $ab \rightarrow cd$ subreaction kinematics through $\hat{s} = x_a x_b s$, $\hat{t} = x_a t/z$, $\hat{u} = x_b u/z$ with $s = (p_A + p_B)^2$, $t = (p_A - p_C)^2$, $u = (p_B - p_C)^2$. The conditions $\hat{s} + \hat{t} + \hat{u} = 0$ and $z = x_1/x_a + x_2/x_b \leq 1$ fix the lower limits of integration at

$$x_a^{\min} = \frac{x_1}{1 - x_2}, \quad x_b^{\min} = \frac{x_a x_2}{x_a - x_1}$$

with $x_1 = -u/s$ and $x_2 = -t/s$. The parton distributions are denoted by $P_{a/A}(x_a, Q^2)$ representing the probability for the constituent a of the hadron A to have fractional longitudinal momentum x_a , i.e., $P_{u/p}(x_a, Q^2) \equiv u(x_a, Q^2)$, etc. Similarly the fragmentation functions $D_{C/c}$ describe the probability that the constituent c decays into a hadron C carrying fractional momentum z . The dependence of these distributions on Q^2 refer to their appropriate scaling violations.

The expressions for $d\sigma/d\hat{t}$ in Eq. (1) for the various subprocesses are summarized in the Appendix. The strong running coupling constant is fixed by four-flavor QCD,

$$\alpha_s(Q^2) = \frac{12\pi}{25 \ln(Q^2/\Lambda^2)} \quad (2)$$

with $\Lambda \approx 0.5$ GeV. (For the present purpose contributions from subprocesses involving charmed quarks are entirely negligible because of the smallness of the charm sea.) Apart from elastic scattering of unlike quarks, the choice of Q^2 is in general not unique. This follows from the fact that, for processes involving vector gluons, gauge invariance requires all crossed-channel diagrams to contribute with *equal* couplings regardless of the momentum carried by the internal propagators. This arbitrariness, however, does not drastically

influence the predictions for total single-particle yields²⁰ going, for example, from $Q^2 = (\hat{s}\hat{t}\hat{u})^{1/3}$ to $Q^2 = (\hat{s}-\hat{t}-\hat{u})/3$, $-\hat{t}$, or \hat{s} typically changes the final result by not more than $\pm 20\%$. For definiteness, we choose $Q^2 = -\hat{t}$ as suggested by hard quark-quark scattering.

A. Parton distributions

In order to show the dependence of the predictions of Eq. (1) on various quark and gluon distributions as well as the effects stemming from scaling violations in parton densities, and possibly also in fragmentation functions, we shall employ three different sets of parametrizations:

(i) The parametrization of Barger and Phillips²² combined with a gluon distribution in the nucleon dictated by counting rules¹⁸

$$xG(x) = 3(1-x)^5, \quad (3)$$

where the normalization has been determined by requiring that gluons carry 50% of the nucleon's momentum. This parametrization represents the *naive* quark-parton model [Q^2 -independent $P_{a/A}$'s in Eq. (1)] which, together with the rather flat gluon density of Eq. (3), will roughly yield an *upper* limit for the production of large- p_T hadrons.

(ii) The parton distributions of Buras and Gaemers⁹ with the scaling deviations as predicted by QCD, where the input densities at $Q^2 = Q_0^2 = 1.8$ GeV² have been obtained from fits to deep-inelastic $e(\mu)p$ data. For the valence distributions we have used the simple parametrization of the QCD predicted Q^2 dependence as given in Ref. 9, whereas we have smoothly interpolated the parameters of Table 2 of Ref. 9 to obtain the Q^2 dependence of the sea and gluon distributions in the region $1 \leq Q^2 \leq 10^4$ GeV² valid for⁹ $x \leq 0.3$:

$$x\xi(x, Q^2) = \frac{1}{6}(1.210 + 0.613\bar{s} + 0.764\bar{s}^2) \times (1-x)^{1.0+1.652\bar{s}+3.330\bar{s}^2}, \quad (4)$$

$$xG(x, Q^2) = (2.410 + 3.592\bar{s} + 2.393\bar{s}^2) \times (1-x)^{5+7.201\bar{s}+3.887\bar{s}^2}, \quad (5)$$

where

$$\bar{s} = \ln[\ln(Q^2/\Lambda^2)/\ln(Q_0^2/\Lambda^2)].$$

The $SU(3)$ -symmetric noncharmed sea ξ is defined by the usual decomposition $u = u_v + \xi$, $d = d_v + \xi$, $\bar{u} = \bar{d} = s = \bar{s} \equiv \xi$. It should be noted that we have used a gluon input which behaves like $xG(x, Q_0^2) \sim (1-x)^5$, although a $(1-x)^{10}$ input was mainly used in Ref. 9. The reason for this is because a gluon as steep as $(1-x)^{10}$ is in conflict²³ with recent low- x μp Fermilab data.

(iii) Quark and gluon distributions dynamically calculated¹⁷ within the framework of QCD. Although these densities are purely field-theoretic predictions having no free parameters, they might slightly underestimate¹⁷ the gluon and sea content of hadrons. Thus, this set of parton distributions represents one extreme while the (flatter) naive counting rule-like distributions in (i) represent another.

It is not at all obvious that the scaling violations calculated from QCD for electroproduction data are the same as those for high- p_T processes. This is because a photon probes the charge density of a proton, while the gluon probes the color density, and the two densities may not be identical. It seems clear, however, that we cannot ignore the possibility of scaling violations in purely hadronic reactions as well. In the absence of any better knowledge, we can assume that the scaling violations are similar to those observed in lepton processes, with the understanding that there may be large theoretical uncertainty in the application. This appears to be a much more conservative assumption than adopting^{13, 15} a powerlike Q^2 behavior for scaling violations which, being not only in disagreement with QCD, might strongly overestimate the effects of scale breaking.

B. Fragmentation functions

Isopin and charge-conjugation invariance reduces the number of independent $D_{\pi/q}$ fragmentation functions²⁴ to three; these can be further reduced to two by assuming⁴ that $D_{\pi^+/s}$ is approximately equal to $D_{\pi^+/d}$, both of which are unfavored ("sea") with respect to $D_{\pi^+/u}$ since a π^+ can be formed directly from a u by combining with a \bar{d} (produced from a bremsstrahlung gluon which converts into a $d\bar{d}$), whereas to make a π^+ from either d or s requires the creation (via gluon bremsstrah-

lung) of at least two new flavor pairs, $u\bar{u}$ and $d\bar{d}$. Thus we have

$$D_{\pi^+/u} = D_{\pi^-/d} = D_{\pi^-/\bar{u}} = D_{\pi^+/\bar{d}}, \quad (6a)$$

$$D_{\pi^-/u} = D_{\pi^+/d} = D_{\pi^-/\bar{d}} = D_{\pi^+/\bar{u}} \simeq D_{\pi^+/s} = D_{\pi^-/s} = D_{\pi^+/\bar{s}} = D_{\pi^-/\bar{s}}, \quad (6b)$$

and

$$D_{\pi^0/q} = (D_{\pi^+/q} + D_{\pi^-/q})/2$$

for each flavored quark q . Following the same reasoning^{4, 24} the number of independent fragmentation functions for producing K mesons can be reduced to three:

$$D_{K^+/u} = D_{K^0/d} = D_{K^-/\bar{u}} = D_{\bar{K}^0/\bar{d}}, \quad (7a)$$

$$D_{K^-/s} = D_{\bar{K}^0/s} = D_{K^+/\bar{s}} = D_{K^0/\bar{s}}, \quad (7b)$$

$$D_{K^-/u} = D_{\bar{K}^0/d} = D_{K^+/\bar{u}} = D_{K^0/\bar{d}} \simeq D_{K^-/d} = D_{\bar{K}^0/u} = D_{K^+/\bar{d}} = D_{K^0/\bar{u}} \simeq D_{K^+/d} = D_{K^0/u} = D_{K^-/\bar{d}} = D_{\bar{K}^0/\bar{u}} \simeq D_{K^+/s} = D_{K^0/s} = D_{K^-/\bar{s}} = D_{\bar{K}^0/\bar{s}}. \quad (7c)$$

Furthermore, we expect⁴ that

$$D_{K^+/\bar{s}}/D_{\pi^+/\bar{d}} = D_{K^-/s}/D_{\pi^+/u} - 1$$

as $z \rightarrow 1$ and

$$D_{K^+/u}/D_{K^+/\bar{s}} = D_{K^+/u}/D_{K^-/s} - 1$$

as $z \rightarrow 0$. All these constraints are satisfied by the simple ansatz

$$zD_{\pi^+/u} = a\sqrt{z}(c-z) + \xi_\pi(1-z)^2, \quad zD_{\pi^-/u} = \xi_\pi(1-z)^2, \\ zD_{K^+/u} = b\sqrt{z}(c-z) + \xi_K(1-z)^2, \quad zD_{K^-/u} = \xi_K(1-z)^2, \\ zD_{K^-/s} = a\sqrt{z}(c-z) + \xi_K(1-z)^2, \quad (8)$$

where, analogously to parton distributions, we have decomposed the favored fragmentation functions into "valence" ($\sim\sqrt{z}$) and "sea" components. This ansatz is intuitively plausible as can be seen from the following argument. As $z \rightarrow 0$ more and more $q\bar{q}$ pairs are produced via gluon bremsstrahlung off the original outgoing quark. Thus, most of the observed mesons will come from a combination of a q and \bar{q} from this gluon produced sea. Alternatively, for $z \rightarrow 1$ many fewer $q\bar{q}$ pairs can be produced and therefore the original outgoing quark will dominantly participate in forming the observed meson. These two mechanisms are referred to as the "sea" and "valence" terms, respectively. It should also be noted that the data^{25, 26} on the $\nu(\bar{\nu})$ induced ratio π^+/π^- (π^-/π^+) dictate $D_{\pi^-/u}/D_{\pi^+/u}$ to behave roughly as $(1-z)^1$ which implies for the "sea" components in Eq. (8) a $(1-z)^2$ behavior. This is in disagreement with naive counting rules where one expects^{18, 3} $zD_{\pi^-/u} \sim (1-z)^5$ for example. As $z \rightarrow 1$ the ratio $D_{K^-/u}/D_{\pi^-/u}$ is a direct measure for

SU(3) breaking: We expect $\xi_K/\xi_\pi < 1$ since it might be harder to make new $s\bar{s}$ pairs than $u\bar{u}$ pairs for large z because of the mass of the s quark. We have no way to guess at the amount of this SU(3) breaking but have chosen for definiteness

$$\xi_K/\xi_\pi = \frac{1}{2}. \quad (9)$$

Our results are rather insensitive to this choice and semi-inclusive lepton-nucleon data are even consistent with $\xi_K = \xi_\pi$. Furthermore, data for the production of charged hadrons in deep-inelastic neutrino interactions suggest, as will be discussed below, the following constraint at $z = 1$:

$$(a+b)(c-1) \approx 0.075. \quad (10)$$

It should be noted that the lepton data²⁶⁻³² are not entirely consistent with each other in the region near $z \approx 1$. While some data suggest a value for the right-hand side of Eq. (10) as large as 0.2, other data suggest a value of zero.³¹ This leads to some uncertainty in the normalization of the high- p_T predictions since the present data are sensitive to $z \approx 0.8$. The value adopted here is a conservative estimate based on the data shown in Figs. 1-3.

Further constraints on the remaining three parameters in Eq. (8) come from the momentum-conservation sum rules

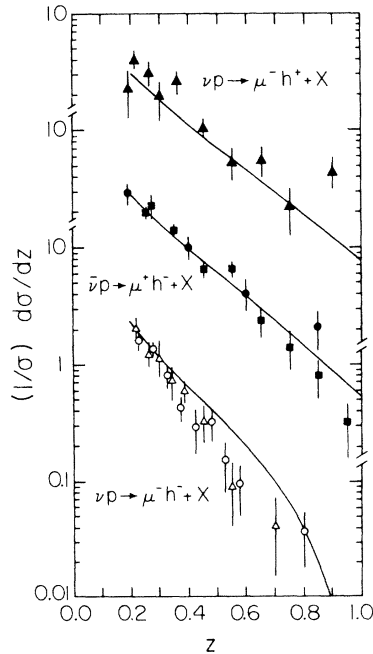


FIG. 1. Comparison of the results of our fragmentation function parametrizations, Eq.(8), with data for charged hadron multiplicity distributions measured in deep-inelastic neutrino scattering. The data are taken from Ref. 26 (●, ○), Ref. 27 (■), and Ref. 28 (▲, △).

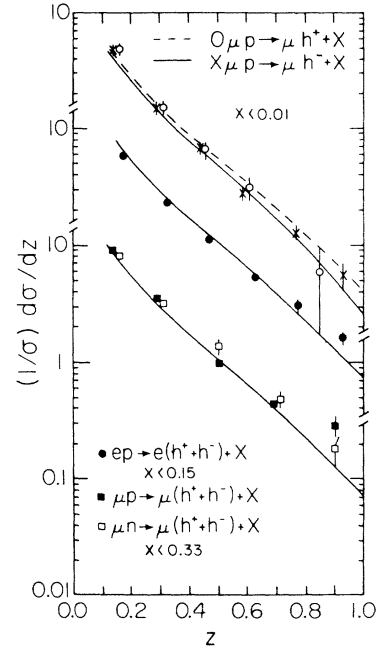


FIG. 2. Comparison of our fragmentation functions with charged-hadron multiplicities measured in deep-inelastic $e(\mu)p$ scattering. Data are from Ref. 29 (●), Ref. 30 (■, □), and Ref. 31 (×, ○).

$$\sum_H \int_0^1 dz z D_{H/q} = 1, \quad (11)$$

which yield two independent constraints, and, in addition, one must satisfy the following isospin

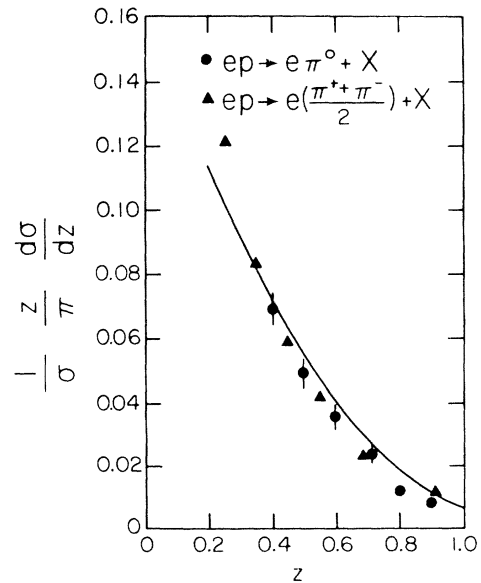


FIG. 3. Comparison of our results with data for π^0 and $(\pi^+ + \pi^-)/2$ electroproduction. The data have been taken from Ref. 32.

sum rule:

$$\int_0^1 dz [(D_{\pi^+ / u} - D_{\pi^- / u}) + \frac{1}{2}(D_{K^+ / u} - D_{K^0 / u}) + \frac{1}{2}(D_{\bar{K}^0 / u} - D_{K^- / u})] = \frac{1}{2}. \quad (12)$$

Solving Eqs. (10)–(12) one obtains for the parameters in Eq. (8)

$$a = \frac{9}{40}, \quad b = \frac{9}{80}, \quad c = \frac{11}{9}, \quad \xi_\pi = \frac{61}{125}. \quad (13)$$

Note that our ansatz in Eq. (8), together with Eqs. (11) and (12), automatically implies $b/a = \frac{1}{2}$, i.e., $D_{K^+ / u} / D_{\pi^+ / u} \rightarrow 0.5$ as $z \rightarrow 1$ as naively expected⁴ from SU(3) breaking and as required by the experimental result^{33,34} that $\sigma(p\bar{p} \rightarrow K^+ X) / \sigma(p\bar{p} \rightarrow \pi^+ X)$ is about 0.5 at large x_T . In addition, our fragmentation functions predict the charge sum rules to be

$$\begin{aligned} \int_0^1 dz (D_{\pi^+ / u} - D_{\pi^- / u} + D_{K^+ / u} - D_{K^- / u}) &= \frac{3}{5}, \\ \int_0^1 dz (D_{\pi^+ / d} - D_{\pi^- / d} + D_{K^+ / d} - D_{K^- / d}) &= -\frac{2}{5}, \quad (14) \\ \int_0^1 dz (D_{\pi^+ / s} - D_{\pi^- / s} + D_{K^+ / s} - D_{K^- / s}) &= -\frac{2}{5} \end{aligned}$$

instead of $\frac{2}{3}$, $-\frac{1}{3}$, and $-\frac{1}{3}$, respectively, as one might naively expect. This is in agreement with the (fitted) results of Ref. 4, and with expectations³⁵ based on a small leakage of quark charges through the hadronic plateau due to SU(3) breaking.

Having determined the quark fragmentation functions, the only remaining unknowns are the gluon decay functions. In any consistent field-theoretic model where $q\bar{q}$ pairs are produced via gluons emitted by the initial quark, the gluon fragmentation function $D_{H/g}(z)$ must be steeper than the favored "valence" component of the quark decay functions, and flatter than the unfavored "sea" distributions. Guided by Eq. (8) we therefore take

$$zD_{\pi/g} = C_\pi(1-z)^{1.5}, \quad zD_{K/g} = C_K(1-z)^{1.5}, \quad (15)$$

and following Eq. (9) we set $c_K/c_\pi = \frac{1}{2}$. Total momentum conservation

$$\int_0^1 dz z(3D_{\pi/g} + 4D_{K/g}) = 1 \quad (16)$$

yields $c_\pi = \frac{1}{2}$. [Recall that naive counting rules predict, for instance $zD_{\pi/g} \sim (1-z)^3$ whereas $zD_{\pi^+ / u} \sim (1-z)^1$ and $zD_{\pi^- / u} \sim (1-z)^5$ in disagreement with semi-inclusive neutrino data,²⁵⁻²⁸ as discussed above.]

Considerably less is known about scaling deviations in fragmentation functions than in parton distributions. However, field-theoretic arguments³⁶ and model calculations³⁷ have shown that $D(z, Q^2)$ should behave similarly to $P(x, Q^2)$, i.e., D should

fall near $z=1$ and rise near $z=0$ as Q^2 grows; furthermore, it is reasonable to expect D to vary with Q^2 at the same rate for $z \approx 1$ as P does near $x=1$, in agreement with the Gribov-Lipatov reciprocity relation.³⁸ This indicates that it may not be unreasonable to assume that asymptotic freedom corrections to $D(z, Q^2)$ are the same as those for $P(x, Q^2)$, especially for $z \approx 1$ which is the only region of importance for present large- p_T experiments. For purely illustrative reasons we therefore will also give predictions with Q^2 -dependent fragmentation functions using the following QCD formula³⁹ valid near $z=1$:

$$zD(z, Q^2) \simeq zD(z, Q_0^2) e^{0.69G^3} (-\ln z)^p \frac{\Gamma(d+1)}{\Gamma(d+1+p)}, \quad (17)$$

where $G = \frac{4}{25}$, $p = 4G\bar{s}$, and $zD(z, Q_0^2) \approx 3 \text{ GeV}^2 = z^n(1-z)^d$ with $n=0$ or $\frac{1}{2}$.

In Figs. 1–3 data²⁶⁻³² for leptonic production of charged hadrons are compared with the predictions of the fragmentation function parametrization given in Eqs. (8)–(13). The data are plotted in the form of normalized z distributions (multiplicity distributions) where z is the fraction of the available energy carried by the hadron. Specifically, in the laboratory frame $z = E_h/\nu$ where E_h and ν are the hadron energy and the energy transferred to the hadronic system, respectively. An alternative variable, x_F , is often used in presenting data on semi-inclusive lepton scattering. x_F is defined in the hadronic center-of-mass system by $p_{\parallel}^*/p_{\parallel \text{max}}^*$ where p_{\parallel}^* is the longitudinal momentum of the hadron measured along the direction of motion of the incoming virtual photon (or W^*). For forward going hadrons, i.e., $x_F > 0$, $z \approx x_F$. However, for z near zero this relation breaks down since the entire region $x_F \leq 0$ is mapped into a region near $z \geq 0$. For this reason only data for x_F or $z \geq 0.2$ have been used.

Hadron production by neutrinos yields a very direct measurement of the various fragmentation functions. Neglecting the Cabibbo angle, the multiplicity distributions are directly proportional to the appropriate fragmentation functions, independent of the parton distributions in the target nucleons.^{4,24} The curves shown in Fig. 1 represent the sum of charged π and K production since, at this point, data with reliable separation of π 's and K 's are not available. There is also, presumably, some contribution to the h^+ data from proton production, but this is expected to be small, especially in the region near $z=1$. The upper curve is thus a sum of favored fragmentation functions, $D_{\pi^+ / u} + D_{K^+ / u}$, the middle curve is a sum of a favored and an unfavored term, $D_{\pi^- / d} + D_{K^- / d}$, while the lowest curve is a sum of two disfavored contributions,

$D_{\pi^-/u} + D_{K^-/u}$. In each case the parametrization adequately reproduces the data, although the sea terms are somewhat large in the intermediate z region. This is of little consequence, however, since the region needed for the high- p_T predictions is $0.7 \leq z \leq 1.0$. The value of the upper two curves at $z = 1$ is sensitive to the parameter c as shown in Eq. (10). The data do not yield a precise value for this parameter and the choice made here may in fact be an underestimate as will be shown below.

Results for the multiplicity distributions measured in electroproduction and muoproduction are shown in Fig. 2. Here the data do not afford as direct a measure of the fragmentation functions since the parton distributions in the target are needed.^{4,24} The curves given here have been calculated using the Barger and Phillips distributions,²² although the results are not very sensitive to the parton densities chosen. In order to properly describe the data shown in Fig. 2, it is of crucial importance to take into account the x range covered by the experiment. For example, when only small x data are used the π^+ and π^- distributions become nearly identical as shown by the muoproduction data in the upper part of Fig. 2. This is expected in the context of the parton model since, for x near zero, the valence-quark distributions go to zero leaving only the sea quarks, thereby giving equal coefficients for the favored and unfavored fragmentation functions for π^+ and π^- . The data in Fig. 2 are, in general, well described by the parametrization given in Eq. (8). However, the data of Refs. 29 and 30 are underestimated in the region near $z \approx 1$, indicating that the right-hand side of Eq. (10) may be too low. However, the difference may simply be due to diffractive ρ production.²⁹⁻³¹ It should be noted that there are additional data from e^+e^- annihilation, quoted in Ref. 30, which also indicate a large value of the multiplicity distribution near $z \approx 1$ while other e^+e^- data, quoted in Ref. (31), appear to fall off as a power of $(1-z)$.

In Fig. 3 results for π^0 and π^\pm electroproduction³² are compared with our parametrization. Again, the description is good, although the curve may be a slight overestimate in the region near $z \approx 1$.

In the calculation of the fragmentation functions used here, dominance of π 's and K 's has been assumed. Possible contributions from protons, η 's, etc. have not been included. This could lead to a possible overestimate of the π and K fragmentation functions. For this reason a conservative estimate for the parameter c , determined by Eq. (10), was adopted. While this may lead to an underestimate of the fragmentation functions near $z \approx 1$, better and consistent lepton data will be needed before the question can be properly resolved.

III. RESULTS

A. Inclusive single- π production

Figures 4–6 contain the predictions for π production at 90° at the upper end of the ISR energy range. In each instance all lowest-order QCD subprocesses have been included. The various curves differ only in the choice of the input parton distribution functions and in the Q^2 dependences of the fragmentation and distribution functions.

In Fig. 4 the results are compared with data^{23, 40, 41} for π production at $\sqrt{s} = 53$ GeV. For the solid and two dashed curves the dynamically calculated QCD parton distributions of Ref. 17 have been used.⁴² The solid curve corresponds to neglecting any Q^2 dependence in the fragmentation functions. For $p_T \geq 4.5$ GeV/ c this curve gives an excellent description of the data, whereas for smaller p_T values the curve lies below the data. The long dashed curve shows the effect of adding the Q^2 dependence of Eq. (17) to the fragmentation functions. This additional Q^2 dependence results in only a slight modification of the p_T dependence and suppresses the curve by a factor of about 3 for the intermedi-

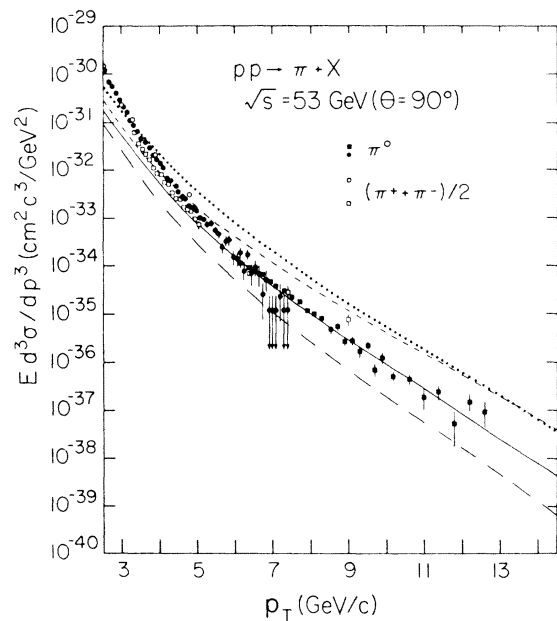


FIG. 4. Comparison of our predictions with the data of Ref. 33 (○), Ref. 40 (●, □), and Ref. 41 (■). The solid curve has been obtained using (Ref. 42) the dynamically calculated QCD parton distributions of Ref. 17 and Q^2 -independent fragmentation functions. For comparison, the results of incorporating the fragmentation-function Q^2 dependence of Eq. (17) are shown by the long-dashed line. The short-dashed and dotted curves were calculated using the Q^2 -independent parton distributions of Ref. 17 and Ref. 22, respectively, so that the only Q^2 dependence is that of the strong running coupling constant α_s .

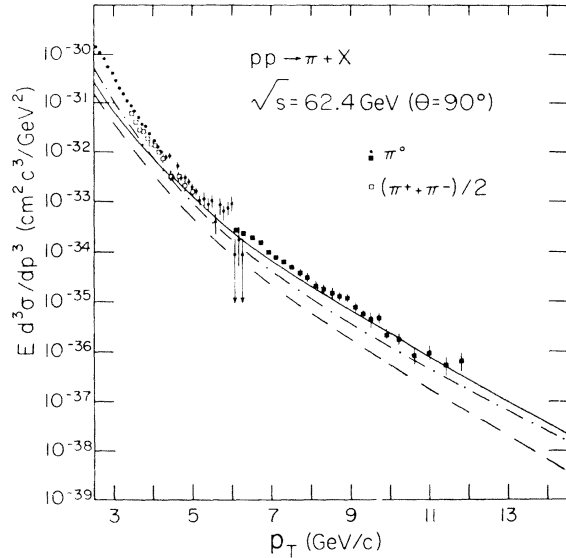


FIG. 5. Comparison of our predictions with the data of Ref. 40 (●, □) and Ref. 41 (■). The solid and long-dashed curves are calculated as in Fig. 4. The results obtained by using the QCD-corrected parton distributions of Ref. 9 are given by the dashed-dotted curve, which may be compared with the solid curve.

ate- p_T range. As noted in Sec. II there is some ambiguity in the π fragmentation functions and those used here represent a conservative lower limit. Therefore, it may be possible to incorpo-

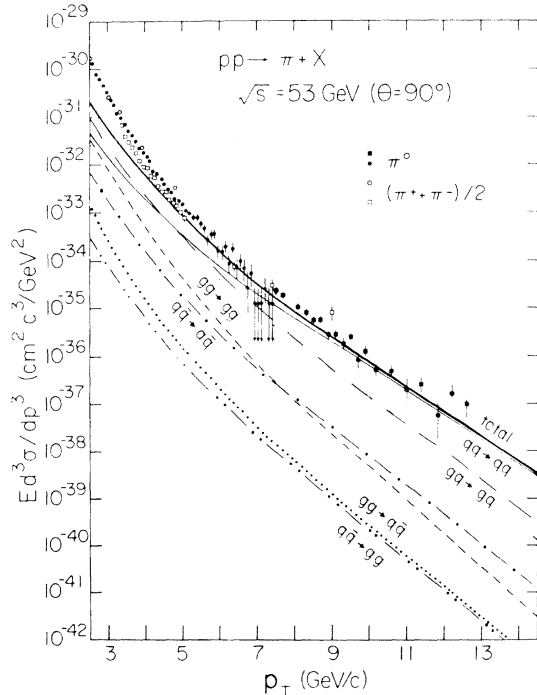


FIG. 6. Individual contributions of the various subprocesses to the solid curve of Fig. 4.

rate some Q^2 dependence into the fragmentation functions. Furthermore, it should be noted that Eq. (17) results from the assumption that the Q^2 dependence of the fragmentation functions can be calculated in the same manner as that of the parton distributions, a plausible but unproved hypothesis.

In contrast, the change in the p_T dependence due to the Q^2 dependence of the distribution functions is quite marked. The short dashed line results from keeping only the Q^2 dependence of the running coupling constant, $\alpha_s(Q^2)$, i.e., the parton distribution and fragmentation functions have all been calculated at $Q^2 = Q_0^2$. Comparing the solid and short dashed curves directly shows the role of the Q^2 dependence of the distribution functions in obtaining the final p_T falloff.

Lastly, the dotted curve has been calculated using the parton distributions of Barger and Phillips²² together with the gluon distribution given in Eq. (3). The only Q^2 dependence is that of the running coupling constant, $\alpha_s(Q^2)$. A comparison of the dotted and short dashed lines then shows the effect of using the flatter gluon of Eq. (3). At small p_T the larger gluon contribution enhances the dotted curve while at larger p_T values the curves converge.

In Fig. 5 data^{40,41} for pion production at $\sqrt{s} = 62.4$ GeV are compared with several theoretical predictions. The solid and dashed lines correspond to the same calculations as in Fig. 4. As before, the solid line provides an excellent description of the data for $p_T \geq 4.5$ GeV/c and lies below the data for smaller p_T . The long dashed curve again lies below the data, due to the extra Q^2 dependence of the fragmentation functions. Also in Fig. 5 the result of using the parton distributions of Ref. 9 is shown by the dashed-dotted line. For this case the fragmentation functions have no Q^2 dependence. Thus, a comparison of the solid and dashed-dotted lines shows the effect of changing just the input parton distribution functions. The differences between the two curves are, in fact, reasonably small over the entire p_T range shown.

The agreement with data for $p_T \approx 2-3$ GeV/c can be further improved by taking into account the internal transverse momenta of the colliding partons. This can lead to an increase of the theoretical predictions of approximately a factor of 2 in this low- p_T region.⁴⁴

The relative importance of the various subprocesses can be discerned by examining Fig. 6. For $p_T \approx 2-3$ GeV/c the dominant subprocess is gluon-quark scattering with gluon-gluon and quark-quark scattering also providing substantial contributions. The three subprocesses $q\bar{q} \rightarrow q\bar{q}$, $g\bar{g} \rightarrow q\bar{q}$, and $q\bar{q} \rightarrow g\bar{g}$ are negligible for all values of p_T

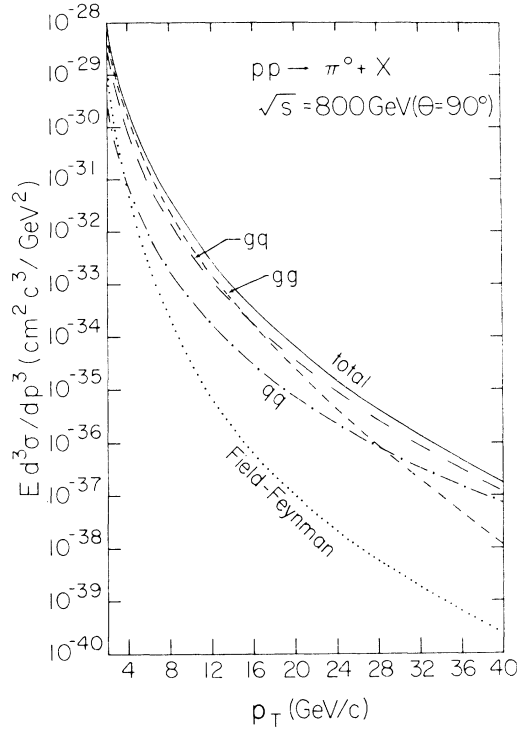


FIG. 7. Predictions for inclusive π^0 production using the Q^2 -dependent parton distributions of Ref. 9. The notation gg denotes the contribution from the sum of the $gg \rightarrow gg$ and $gg \rightarrow q\bar{q}$ subprocess, whereas gq stands for the sum of $gq \rightarrow gq$ and $g\bar{q} \rightarrow g\bar{q}$, and qq refers to the sum of $qq \rightarrow qq$, $q\bar{q} \rightarrow q\bar{q}$, $q\bar{q} \rightarrow gg$, and $\bar{q}q \rightarrow \bar{q}q$. The dotted curve shows the predictions of the model of Ref. 4.

shown here. As p_T increases the gluon-gluon term decreases more rapidly than either the gluon-quark or quark-quark terms. At higher p_T the relative importance of the gluon-quark term also decreases eventually leaving only the quark-quark scattering contribution. This latter term alone scales as p_T^{-4} up to logarithmic terms coming from the Q^2 dependence of the scaling violations and α_s . It is thus clear that the large gluon-gluon and gluon-quark terms are responsible not only for obtaining the correct normalization but also, in part, for obtaining the observed rapid falloff in the intermediate- p_T region.

The gluon-gluon and gluon-quark terms have a stronger energy dependence than the quark-quark scattering term. This may be seen in Fig. 7 where the prediction for $90^\circ \pi^0$ production at a typical ISABELLE energy $\sqrt{s} = 800$ GeV is given. Here the parton distributions of Buras and Gaemers⁹ have been used and the fragmentation functions have no Q^2 dependence. The predictions obtained using the dynamically calculated QCD parton distributions^{17, 42} are very similar, lying about a factor of 1.8 lower for $p_T \lesssim 20$ GeV/c and becoming slightly

larger for $p_T \gtrsim 32$ GeV/c. For $p_T \lesssim 16$ GeV/c the gluon-gluon term dominates followed by the gluon-quark and the quark-quark terms. At larger p_T values the gluon-quark term dominates and, eventually, the quark-quark contribution becomes dominant. This is in contrast to the lower-energy predictions at $\sqrt{s} = 53$ GeV shown in Fig. 6 where the $gq \rightarrow gq$ and $gg \rightarrow gg$ contributions are important only up to $p_T \lesssim 5$ GeV/c. For fixed p_T , the increasing importance of the gluonic contributions for larger \sqrt{s} is due to the decrease in the effective value of $x_T = 2p_T/\sqrt{s}$, thereby probing smaller regions of $x_{a,b}$ in Eq. (1) where the gluon distribution increasingly dominates over the quark distributions. For comparison, the prediction of the Field-Feynman⁴ model is also shown. This curve lies about three orders of magnitude lower than our predicted curve. This is due to two factors, the first of which is that the subprocesses used here all have a p_T^{-4} behavior, up to logarithmic corrections, while the Field-Feynman model scales as p_T^{-8} . Secondly, the large gluon-gluon and gluon-quark contributions further enhance the predicted cross section. The differences shown in Fig. 7 can have a profound effect, for example, on estimates of backgrounds for W^\pm production.

Because of the extremely large values of Q^2 reached at ISABELLE energies, it is of interest to look at the effects of the scaling violations coming from the Q^2 dependence of the various distribution functions. Accordingly, another calculation was done in which only the Q^2 dependence of $\alpha_s(Q^2)$ was retained, i.e., using the Q^2 -independent parton distributions and fragmentation functions. These results show that the inclusion of the scaling violations in the parton distributions increases the cross section by a factor of about 5 at $p_T = 2$ GeV/c, whereas the cross section is unchanged at $p_T \approx 18$ GeV/c and it is decreased by a factor of about 8 at $p_T = 40$ GeV/c. Thus, by going to sufficiently high \sqrt{s} the parton distributions are probed at small enough values of x_T that the expected pattern of scaling violations emerges.

Often in the literature the high- p_T single-particle invariant cross section is parametrized as

$$E \frac{d^3\sigma}{dp^3} = A p_T^{-n} (1 - x_T)^f. \quad (18)$$

The model of Ref. 4 gives $n=8$ by design and the constituent-interchange model, using a quark-hadron scattering subprocess, yields³ $n=8$ and $f=9$. Figure 8 shows our predictions for $p_T^8 E d^3\sigma / dp^3$ for π^0 production at 90° as a function of x_T for $31 \leq \sqrt{s} \leq 800$ GeV. The parton distributions of Ref. 17 have been used.⁴² The cross section has been weighted by a factor p_T^8 so as to afford an easy comparison with the results of the model of

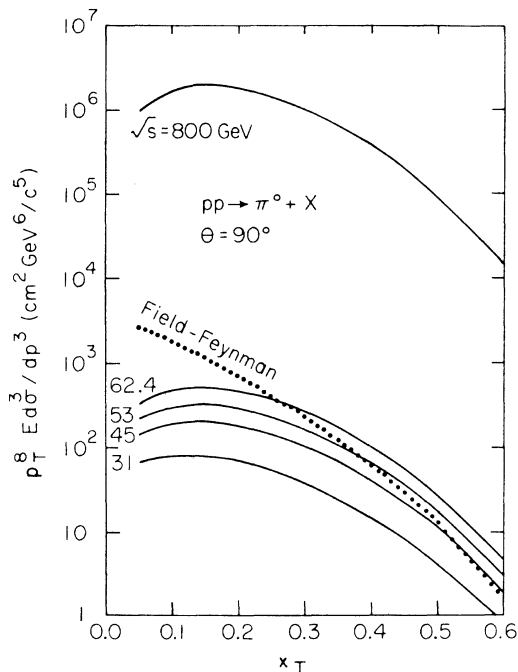


FIG. 8. Predictions for $p_T^8 E d^3 \sigma / dp^3$ for single- π^0 production at 90° . The parton distributions of Ref. 17 were used (see Ref. 42) and no Q^2 dependence was used in the fragmentation functions. The dotted curve shows the results of the model of Ref. 4.

Ref. 4, shown by the dotted line in Fig. 8. The curves shown in Fig. 8 have been fitted to the form given in Eq. (18) and the resulting parameter values are displayed in Table I. Note that neither A , n , nor f is constant as would be expected in a scale-invariant model. The Q^2 dependence of the scaling deviations and of α_s leads not only to a rise in the normalization A , but also to a change in shape, as evidenced by the increase in f . Accordingly, the parametrization of Eq. (18) does not provide a proper description of this QCD calculation. The dramatic difference between a model which scales as p_T^{-8} and the current QCD calculation leads to a decisive test at ISABELLE energies.

Another test of the QCD calculation is to look at

TABLE I. The values for A , n , and f appearing in Eq. (18), as functions of \sqrt{s} .

\sqrt{s} (GeV)	A	n	f
31	119	6.76	8.65
45	163	6.57	8.96
53	192	6.52	9.06
62.4	229	6.48	9.15
800	10 931	6.36	9.52

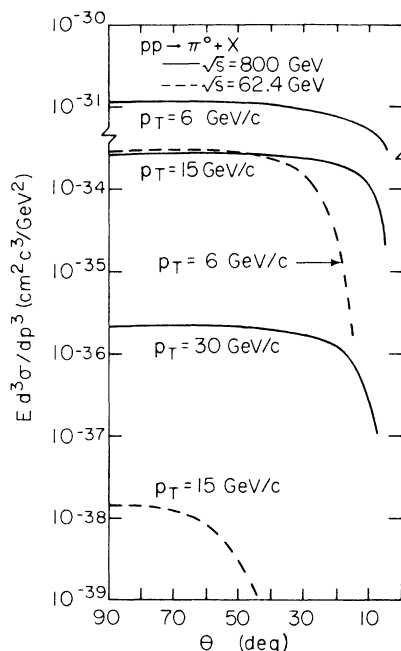


FIG. 9. Predictions for the angular dependence of the invariant cross section for $pp \rightarrow \pi^0 + X$ at several \sqrt{s} and p_T values. The parton distributions of Ref. 17 were used (see Ref. 42) and no Q^2 dependence was used in the fragmentation functions.

the center-of-mass angular dependence at fixed s and p_T . The results are shown at several s and p_T values in Fig. 9. The angular dependence of the model is very flat over a wide range in θ . The turnover at small θ is s dependent and is due to the approach to the kinematic boundary. The minimum allowed value of θ is given by

$$\theta_{\min} = \sin^{-1} 2p_T / \sqrt{s} = \sin^{-1} x_T. \quad (19)$$

This flat angular dependence has been observed in the data and was, in fact, the motivating factor for the choice of $d\sigma/d\hat{t} = A/(-s\hat{t}^3)$ in Ref. 4. Here the QCD predictions agree with the limited data available for $\theta \geq 50^\circ$. However, only the small θ region provides a stringent test for the angular dependence of different models since the prediction of a flat angular distribution for $\theta \geq 50^\circ$ is common to many of them. Unfortunately, no detailed high-energy data exist in the above-mentioned small θ region. In Fig. 10 data⁴⁵ at $\sqrt{s} = 53$ GeV and $\theta = 90^\circ$ and 53° are shown. These data are systematically higher at large p_T and lower at small p_T than the data^{33,40} shown in Figs. 4 and 6, thereby accounting for the apparent change in normalization. Apart from the overall systematic differences, the data show that at small p_T there is a slight rise as θ decreases whereas at $p_T \approx 7$ GeV/c there is no θ dependence. This behavior is exactly re-

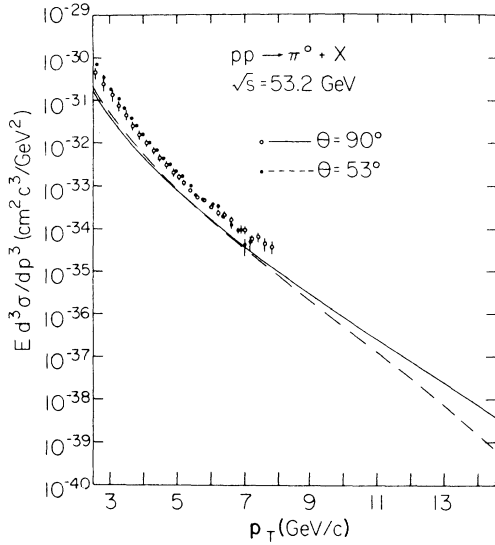


FIG. 10. Comparison of our predictions with the data of Ref. 45. The parton distributions of Ref. 17 were used (see Ref. 42) and the fragmentation functions do not have any Q^2 dependence.

produced by the QCD calculation as shown by the solid ($\theta = 90^\circ$) and dashed ($\theta = 53^\circ$) lines. It is interesting to note that the $qq \rightarrow qq$ contribution has the same general shape as the full calculation, but the magnitude is reduced by a p_T dependent amount

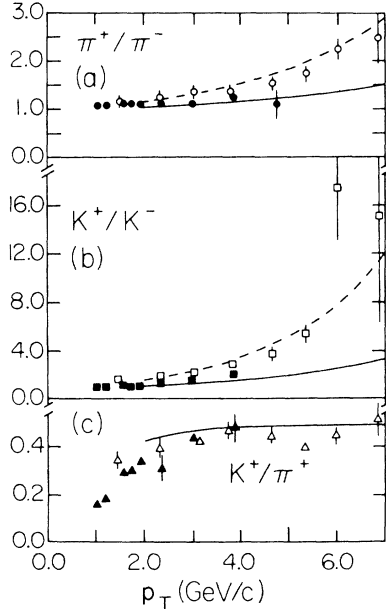


FIG. 11. Comparison of our predictions with the particle ratio data of Ref. 46 ($\circ, \square, \triangle$) at $P_{1ab} = 400$ GeV/c and Ref. 47 ($\bullet, \blacksquare, \blacktriangle$) at $\sqrt{s} = 53$ GeV. Both data sets are for pp reactions. The dashed lines correspond to our predictions at $P_{1ab} = 400$ GeV/c and the solid ones to $\sqrt{s} = 53$ GeV.

with the gluon terms being dominant at the smaller p_T values.

B. Particle ratios

As emphasized in Ref. 4, the study of the cross-section ratios of various single-particle inclusive reactions at high p_T affords an important test of the fragmentation functions, which is relatively insensitive to the underlying subprocesses or to the input parton distributions. The results of the QCD calculation are shown in Fig. 11 for two sets of energies. As can be seen, the agreement with the data^{46, 47} is in all cases very good. This may seem somewhat surprising since at $\sqrt{s} = 27$ GeV the absolute normalization is too low and the p_T dependence for $p_T \lesssim 4$ GeV/c is too flat. However, these differences tend to cancel in the ratios, and therefore the ratios are most sensitive to the fragmentation functions. Note that inclusion of parton transverse momentum effects will yield better agreement with the cross-section data at lower energies and smaller p_T values. However, the particle ratios should be insensitive to these effects.

The energy dependence shown by the π^+/π^- and K^+/K^- ratios is easy to understand since both the data and the model curves approximately scale in x_T . For example, compare the $p_T = 6$ -GeV/c points at $\sqrt{s} = 53$ GeV/c with the 3-GeV/c points at $\sqrt{s} = 27$ GeV, which corresponds to a fixed $x_T \approx 0.023$. The K^+/π^+ ratio is virtually energy independent over the range shown. The value of about 0.5 is a direct consequence of the ratio of $b/a = 0.5$, see Eq. (8), as discussed in Sec. II.

Although the behavior of the ratios is dominated by the fragmentation functions, the gluon-gluon and gluon-quark subprocesses do play a role in determining the p_T dependence of the π^+/π^- and K^+/K^- ratios. At small p_T the gluon-related terms are important and tend to drive the two ratios toward 1. In this regard, our predictions for these two ratios tend to lie lower than the predictions of Field and Feynman at small p_T , in better agreement with the data. At higher p_T values the gluon contributions become less important and the behavior becomes characteristic of the underlying quark-quark subprocess. The ratios rise since there are more u quarks than d quarks and at large z $D_{\pi^+ / u} > D_{\pi^- / u}$ and $D_{K^+ / u} > D_{K^- / u}$. Note that in this regard $D_{\pi^+ / g} = D_{\pi^- / g}$ and $D_{K^+ / g} = D_{K^- / g}$ leading to a ratio of one for the gluon-dominated terms, as discussed above.

IV. SUMMARY AND CONCLUSIONS

The calculations presented here demonstrate that within the framework of QCD it is possible to predict both the normalization and the p_T depen-

dence of the hadronic single-particle inclusive data in the ISR range for $p_T \gtrsim 4.5$ GeV/c. This can be done without any free parameters, using as input only the quark and gluon fragmentation and distribution functions determined in analyses of leptonic data. These results show that it is of crucial importance to take into account all lowest-order diagrams allowed in QCD. In particular, the inclusion of the large gluon-gluon term has a profound effect on both the normalization and the p_T dependence of the predictions.

The improved agreement with the data obtained here can be traced to several factors. The large gluon-gluon and gluon-quark contributions substantially increase the magnitude of the predicted cross section at moderate p_T values. The rapid falloff with p_T of these contributions leads to an overall p_T behavior which is in better agreement with the data than that which results from the quark-quark scattering term alone. In addition, the Q^2 dependence of the various distribution functions further enhances the p_T falloff. The effects of these scaling violations become particularly striking in the ISABELLE energy range, due to the larger Q^2 range covered. Here scaling violations significantly steepen the p_T dependence of cross sections by increasing (decreasing) them at low (high) values of p_T . Additional Q^2 dependence may be contained in the fragmentation functions. However, over the currently accessible Q^2 region these effects show up mostly as a shift in the overall normalization, with only a slight modification of the p_T dependence.

At ISABELLE energies, the inclusion of gluon-related terms together with the p_T^{-4} behavior of the individual subprocesses results in a π^0 -production cross section which is up to three orders of magnitude larger than the predictions of the phenomenological model of Field and Feynman.⁴ Thus, the difference between these two models will be easily discernable. In addition, this large cross section can have a significant effect on background estimates for W^\pm production.

This analysis has shown that it is possible, within the framework of QCD, to *predict* the correct angular dependence of the cross section for $pp \rightarrow \pi^0 + X$ at ISR energies. Furthermore, the model correctly predicts the π^+/ π^- , K^+/K^- , and K^+/ π^+ cross-section ratios over a wide range in both \sqrt{s} and p_T . These results indicate that for $\sqrt{s} \gtrsim 50$ GeV and $p_T \gtrsim 4.5$ GeV/c the lowest-order QCD calculation is able to properly describe the single-particle inclusive data. Furthermore, the inclusion of effects due to parton transverse momenta may well allow the region of validity of these calculations to be extended even further.

Note added. Meanwhile, two publications have ap-

peared where in addition to gluonic QCD contributions, possible effects due to parton transverse momenta are studied [R. D. Field, Phys. Rev. Lett. **40**, 997 (1978); A. P. Contogouris, R. Gaskell, and S. Papadopoulos, Phys. Rev. D **17**, 2314 (1978)].

ACKNOWLEDGMENTS

One of us (M. G.) would like to thank B. L. Combridge and J. F. Gunion for some useful remarks concerning the $gg \rightarrow gg$ cross section. J. F. O. wishes to thank A. P. Contogouris and J. Ranft for several interesting discussions. This work was supported in part by the U. S. Energy Research and Development Administration.

APPENDIX

The differential cross sections for the (massless) hard-collision subprocesses in Eq. (1) can be written, to lowest order in QCD, as

$$\frac{d\sigma^{ab \rightarrow cd}}{dt} = \frac{\pi \alpha_s^2}{s^2} \Sigma^{ab \rightarrow cd} \quad (\text{A1})$$

where the invariants s, t, u are defined as usual and satisfy $s + t + u = 0$. Note that these invariants here refer to the quark and gluon subprocesses and should not be confused with $s = (p_A + p_B)^2$, etc., in Eq. (1), but should be identified with \hat{s} , \hat{t} , and \hat{u} of Sec. II. For completeness we will summarize the results²⁰ for the various cross sections appearing in Eq. (A1).

The cross section for elastic gluon-gluon scattering, $gg \rightarrow gg$, is determined from the gauge invariant s, t, u , and contact Feynman diagrams. The various polarization sums corresponding to the incoming and outgoing vector gluons can be evaluated by using the appropriate projection operators²¹ for the transverse polarization states, i.e.,

$$\begin{aligned} \sum_{\text{spins}} \epsilon_1^\mu \epsilon_1^{\nu*} &= -g^{\mu\nu} + \frac{2}{s} (k_1^\mu k_2^\nu + k_2^\mu k_1^\nu) \\ &= \sum_{\text{spins}} \epsilon_2^\mu \epsilon_2^{\nu*}, \end{aligned} \quad (\text{A2})$$

where $k_1(\epsilon_1) + k_2(\epsilon_2) \rightarrow k_3(\epsilon_3) + k_4(\epsilon_4)$. A similar expression holds for the sums over the outgoing gluon polarization vectors. It should be noted that, contrary to QED, one must *not* make the Feynman-gauge replacement $\Sigma \epsilon^\mu \epsilon^{\nu*} = -g^{\mu\nu}$ since $k_1^\mu T_{\mu\nu\lambda\sigma} \neq 0$, although the gauge invariance condition on the scattering amplitude reads as usual

$$k_1^\mu \epsilon_2^\nu \epsilon_3^\lambda \epsilon_4^\sigma T_{\mu\nu\lambda\sigma} = 0. \quad (\text{A3})$$

Using Eq. (A2) or doing the polarization sums "by hand" by using explicit helicity amplitudes, a somewhat lengthy calculation yields

$$\Sigma^{gg \rightarrow gg} = \frac{9}{2} \left(3 - \frac{tu}{s^2} - \frac{su}{t^2} - \frac{st}{u^2} \right), \quad (\text{A4})$$

which is in agreement with the recently published result of Ref. 20. The cross section for $gg \rightarrow q\bar{q}$ has been calculated in Refs. 19 and 20, and is given by

$$\Sigma^{gg \rightarrow q\bar{q}} = \frac{1}{6} \left(\frac{t}{u} + \frac{u}{t} \right) - \frac{3}{8} \frac{t^2 + u^2}{s^2}, \quad (\text{A5})$$

from which we obtain the cross section for $q\bar{q} \rightarrow gg$ by just taking into account the different color averaging of the initial state, i.e., multiplying Eq. (A5) by a factor of $\frac{64}{9}$:

$$\Sigma^{q\bar{q} \rightarrow gg} = \frac{32}{27} \left(\frac{t}{u} + \frac{u}{t} \right) - \frac{8}{3} \frac{t^2 + u^2}{s^2}. \quad (\text{A6})$$

Similarly, the reaction $gq \rightarrow gq$ follows from Eq. (A5) by $s \leftrightarrow t$ crossing and by multiplying (A5) by a factor of $\frac{8}{3}$ for the average over the ingoing gluon and quark colors:

$$\Sigma^{gq \rightarrow gq} = -\frac{4}{9} \left(\frac{s}{u} + \frac{u}{s} \right) + \frac{s^2 + u^2}{t^2}, \quad (\text{A7})$$

which, by time-reversal invariance, is equal to the cross section for $g\bar{q} \rightarrow g\bar{q}$.

Finally, it is straightforward to calculate the various quark-quark scattering processes^{20, 21}

which have to be equal to the relevant expressions of conventional QED⁴⁸ supplemented by the appropriate color factors. The cross section for the scattering of flavor-unlike quarks (t -channel gluon exchange only) $q_a q_b \rightarrow q_a q_b$ is given by

$$\Sigma^{q_a q_b \rightarrow q_a q_b} = \frac{4}{9} \frac{s^2 + u^2}{t^2} \quad (\text{A8})$$

which is the same for $q_a \bar{q}_b \rightarrow q_a \bar{q}_b$. The process $q_a q_b \rightarrow q_b q_a$ is then simply given by Eq. (A8) with $t \leftrightarrow u$. The scattering for flavorlike quarks $q_a q_a \rightarrow q_a q_a$, where t and u channels contribute, reads

$$\Sigma^{q_a q_a \rightarrow q_a q_a} = \frac{4}{9} \left(\frac{s^2 + u^2}{t^2} + \frac{s^2 + t^2}{u^2} \right) - \frac{8}{27} \frac{s^2}{tu}. \quad (\text{A9})$$

Of course, the results for $q\bar{q} \rightarrow q\bar{q}$ for unlike and like antiquarks equal Eq. (A8) and (A9), respectively. The process $q_a \bar{q}_a \rightarrow q_a \bar{q}_a$ (same flavor and antiflavor) follows from (A9) under $s \leftrightarrow u$ crossing,

$$\Sigma^{q_a \bar{q}_a \rightarrow q_a \bar{q}_a} = \frac{4}{9} \left(\frac{s^2 + u^2}{t^2} + \frac{u^2 + t^2}{s^2} \right) - \frac{8}{27} \frac{u^2}{ts}, \quad (\text{A10})$$

whereas the annihilation process $q_a \bar{q}_a \rightarrow q_b \bar{q}_b$ is just the s -channel contribution to Eq. (A10), i.e.,

$$\Sigma^{q_a \bar{q}_a \rightarrow q_b \bar{q}_b} = \frac{4}{9} \frac{u^2 + t^2}{s^2}. \quad (\text{A11})$$

*Permanent address: Institut für Physik, Universität Mainz, 6500 Mainz, West Germany.

¹S. M. Berman, J. D. Bjorken, and J. B. Kogut, Phys. Rev. D **4**, 3388 (1971).

²S. D. Ellis and M. B. Kislinger, Phys. Rev. D **9**, 2027 (1974).

³R. Blankenbecker and S. J. Brodsky, Phys. Rev. D **10**, 2973 (1974); R. Blankenbecker, S. J. Brodsky, and J. F. Gunion, *ibid.* **12**, 3469 (1975); S. J. Brodsky, Invited talk presented at the VIII International Symposium on Multiparticle Dynamics, Kayserberg, France, 1977, SLAC Report No. SLAC-PUB-2009 (unpublished).

⁴R. D. Field and R. P. Feynman, Phys. Rev. D **15**, 2590 (1977).

⁵G. Parisi and R. Petronzio, Phys. Lett. **62B**, 331 (1976).

⁶M. Glück and E. Reya, Phys. Rev. D **14**, 3034 (1976); Phys. Lett. **64B**, 169 (1976); Phys. Rev. D **16**, 3242 (1977).

⁷A. De Rújula, H. Georgi, and H. D. Politzer, Ann. Phys. (N.Y.) **103**, 315 (1977).

⁸I. Hinchliffe and C. H. Llewellyn Smith, Nucl. Phys. **B128**, 93 (1977).

⁹A. J. Buras and K. J. F. Gaemers, Nucl. Phys. **B132**, 249 (1978).

¹⁰H. Fritzsch, M. Gell-Mann, and H. Leutwyler, Phys. Lett. **47B**, 365 (1973).

¹¹M. Glück and E. Reya, Phys. Lett. **69B**, 77 (1977), and

last reference in Ref. 6.

¹²R. F. Cahalan, K. A. Geer, J. Kogut, and L. Susskind, Phys. Rev. D **11**, 1199 (1975).

¹³R. C. Hwa, A. J. Spiessbach, and M. J. Teper, Phys. Rev. Lett. **36**, 1418 (1976); Phys. Rev. D **18**, 1475 (1978).

¹⁴A. P. Contogouris, R. Gaskell, and A. Nicolaidis, Phys. Rev. D **17**, 839 (1978).

¹⁵R. Cutler and D. Sivers, Phys. Rev. D **16**, 679 (1977).

¹⁶T. Eichten *et al.*, Phys. Lett. **46B**, 274 (1973); H. Denner *et al.*, Nucl. Phys. **B85**, 269 (1975).

¹⁷M. Glück and E. Reya, Nucl. Phys. **B130**, 76 (1977).

These dynamically calculated distributions might slightly underestimate the gluon and sea content of the hadrons due to the fact that the calculation rests on the assumption that at low resolution energies hadrons consist of valence quarks only.

¹⁸G. R. Farrar, Nucl. Phys. **B77**, 429 (1974); J. F. Gunion, Phys. Rev. D **10**, 242 (1974).

¹⁹M. Glück, J. F. Owens, and E. Reya, Phys. Rev. D **17**, 2324 (1978).

²⁰B. L. Combridge, J. Kripfganz, and J. Ranft, Phys. Lett. **70B**, 234 (1977).

²¹R. Cutler and D. Sivers, Phys. Rev. D **17**, 196 (1978).

It should be noted that the constant multiplying the $9\pi\alpha_s^2/2s^2$ in the $gg \rightarrow gg$ cross section stated there equals 51/16 whereas the correct result is 3. The numerical results are known to be insensitive to this

- small discrepancy.
- ²²V. Barger and R. J. N. Phillips, Nucl. Phys. B73, 269 (1974).
- ²³M. Glück and E. Reya, Phys. Lett. 72B, 326 (1978).
- ²⁴M. Gronau, F. Ravndal, and Y. Zarmi, Nucl. Phys. B51, 611 (1973).
- ²⁵M. Haguenaer, in *Proceedings of the XVII International Conference on High Energy Physics, London, 1974*, edited by J. R. Smith (Rutherford Lab., Chilton, Didcot, Berkshire, England, 1974), p. IV-95.
- ²⁶B. P. Roe, in *Proceedings of the 1975 International Symposium on Lepton and Photon Interactions at High Energies, Stanford, California*, edited by W. T. Kirk (SLAC, Stanford, 1976), p. 551.
- ²⁷M. Derrick *et al.*, Phys. Rev. D 17, 1 (1978).
- ²⁸Additional neutrino data have been obtained from Ref. 4.
- ²⁹J. T. Dakin *et al.*, Phys. Rev. D 10, 1401 (1974).
- ³⁰C. del Papa *et al.*, Phys. Rev. D 17, 2843 (1978).
- ³¹L. Hand, in *International Symposium on Lepton and Photon Interactions at High Energies, Hamburg, 1977*, edited by F. Gutbrod (DESY, Hamburg, 1978).
- ³²Ch. Berger *et al.*, Phys. Lett. 70B, 471 (1977).
- ³³B. Alper *et al.*, Nucl. Phys. B100, 237 (1975).
- ³⁴D. Antreasyan *et al.*, Phys. Rev. Lett. 38, 115 (1977).
- ³⁵G. R. Farrar and J. L. Rosner, Phys. Rev. D 10, 2226 (1974).
- ³⁶A. M. Polyakov, in *Proceedings of the 1975 International Symposium on Lepton and Photon Interactions at High Energies, Stanford, California*, edited by W. T. Kirk (SLAC, Stanford, 1976), p. 855.
- ³⁷A. H. Mueller, Phys. Rev. D 9, 963 (1974); C. G. Callan and M. L. Goldberger, *ibid.* 11, 1542 (1975); 11, 1553 (1975); N. Coote, *ibid.* 11, 1611 (1975).
- ³⁸V. N. Gribov and L. N. Lipatov, Yad. Fiz. 15, 1218 (1972) [Sov. J. Nucl. Phys. 15, 675 (1972)].
- ³⁹D. J. Gross, Phys. Rev. Lett. 32, 1071 (1974).
- ⁴⁰F. W. Büsser *et al.*, Nucl. Phys. B106, 1 (1976).
- ⁴¹B. G. Pope, in *Particles and Fields — 1977*, Proceedings of the Meeting of the APS Division of Particles and Fields, edited by P. A. Schreiner, G. H. Thomas, and A. B. Wicklund (AIP, New York, 1978), p. 239.
- ⁴²The parametrization in Ref. 17 is valid for $Q^2 \lesssim 250$ (GeV/c)². An alternative parametrization (see Ref. 43) of the same dynamically calculated distributions, which is valid over a much larger Q^2 region, was therefore used for these calculations.
- ⁴³J. F. Owens and E. Reya, Phys. Rev. D 17, 3003 (1978).
- ⁴⁴R. P. Feynman, R. D. Field, and G. C. Fox, Nucl. Phys. B128, 1 (1977); M. Fontannaz and D. Schiff, *ibid.* B132, 457 (1978).
- ⁴⁵K. Eggert *et al.*, Nucl. Phys. B128, 49 (1975).
- ⁴⁶D. Antreasyan *et al.*, Phys. Rev. Lett. 38, 112 (1977); 38, 115 (1977).
- ⁴⁷B. Alper *et al.*, Nucl. Phys. B87, 19 (1975).
- ⁴⁸See, for example, V. B. Berestetskii, E. M. Lifshitz, and L. P. Pitaevskii, *Relativistic Quantum Theory* (Pergamon, Oxford, 1971), pp. 273–275.

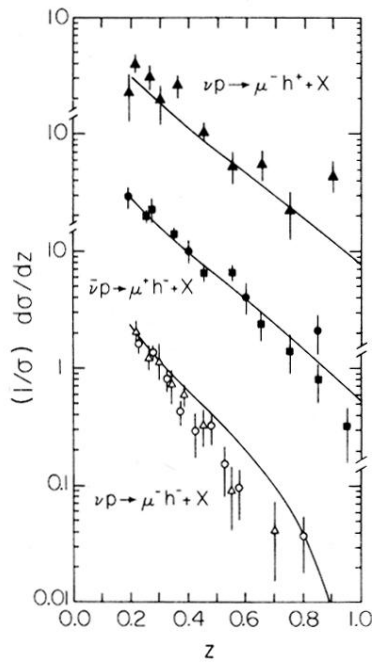


FIG. 1. Comparison of the results of our fragmentation function parametrizations, Eq.(8), with data for charged hadron multiplicity distributions measured in deep-inelastic neutrino scattering. The data are taken from Ref. 26 (●, ○), Ref. 27 (■), and Ref. 28 (▲, △).

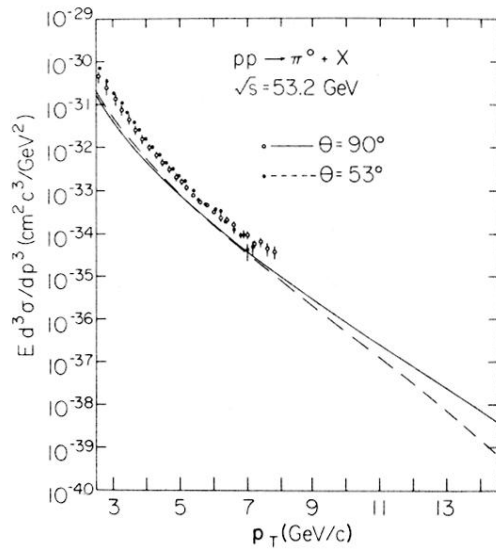


FIG. 10. Comparison of our predictions with the data of Ref. 45. The parton distributions of Ref. 17 were used (see Ref. 42) and the fragmentation functions do not have any Q^2 dependence.

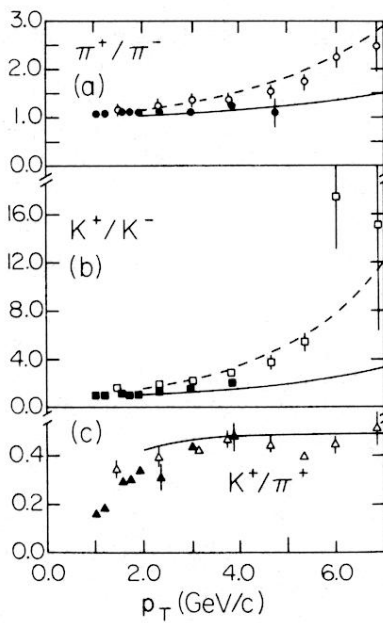


FIG. 11. Comparison of our predictions with the particle ratio data of Ref. 46 ($\circ, \square, \triangle$) at $P_{1ab} = 400$ GeV/c and Ref. 47 ($\bullet, \blacksquare, \blacktriangle$) at $\sqrt{s} = 53$ GeV. Both data sets are for pp reactions. The dashed lines correspond to our predictions at $p_{1ab} = 400$ GeV/c and the solid ones to $\sqrt{s} = 53$ GeV.

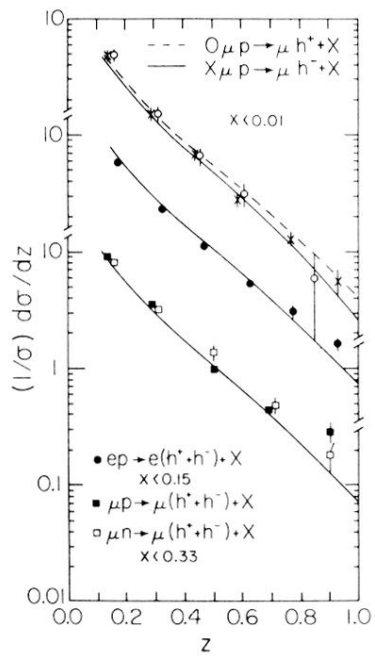


FIG. 2. Comparison of our fragmentation functions with charged-hadron multiplicities measured in deep-inelastic $e(\mu)p$ scattering. Data are from Ref. 29 (●), Ref. 30 (■, □), and Ref. 31 (×, ○).

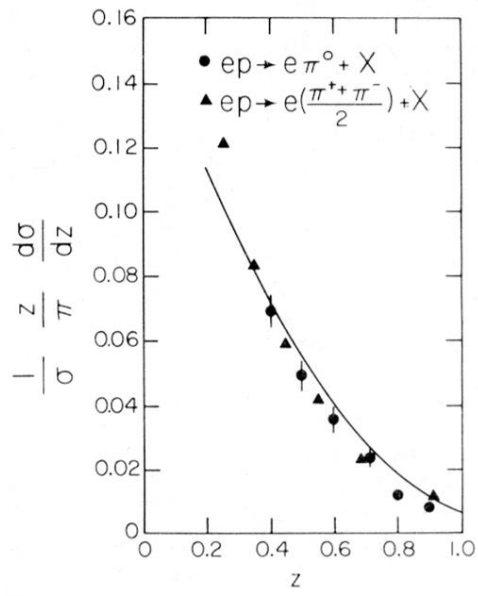


FIG. 3. Comparison of our results with data for π^0 and $(\pi^+ + \pi^-)/2$ electroproduction. The data have been taken from Ref. 32.

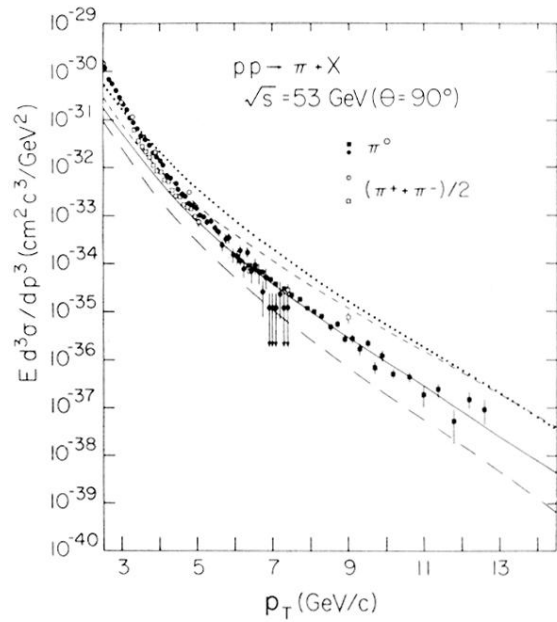


FIG. 4. Comparison of our predictions with the data of Ref. 33 (\circ), Ref. 40 (\bullet, \square), and Ref. 41 (\blacksquare). The solid curve has been obtained using (Ref. 42) the dynamically calculated QCD parton distributions of Ref. 17 and Q^2 -independent fragmentation functions. For comparison, the results of incorporating the fragmentation-function Q^2 dependence of Eq.(17) are shown by the long-dashed line. The short-dashed and dotted curves were calculated using the Q^2 -independent parton distributions of Ref. 17 and Ref. 22, respectively, so that the only Q^2 dependence is that of the strong running coupling constant α_s .

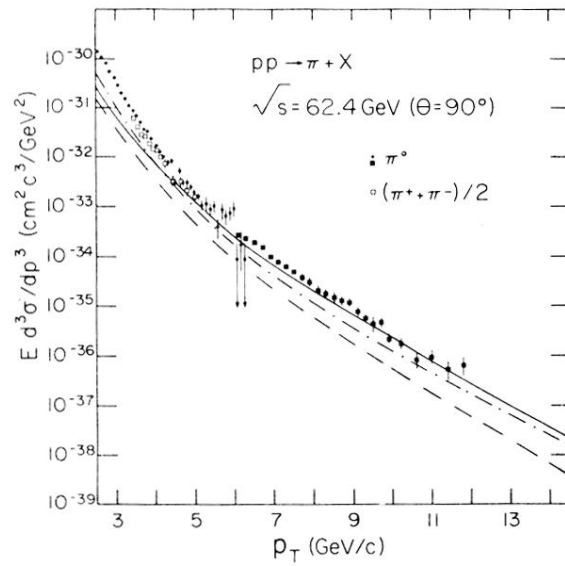


FIG. 5. Comparison of our predictions with the data of Ref. 40 (\bullet , \square) and Ref. 41 (\blacksquare). The solid and long-dashed curves are calculated as in Fig. 4. The results obtained by using the QCD-corrected parton distributions of Ref. 9 are given by the dashed-dotted curve, which may be compared with the solid curve.

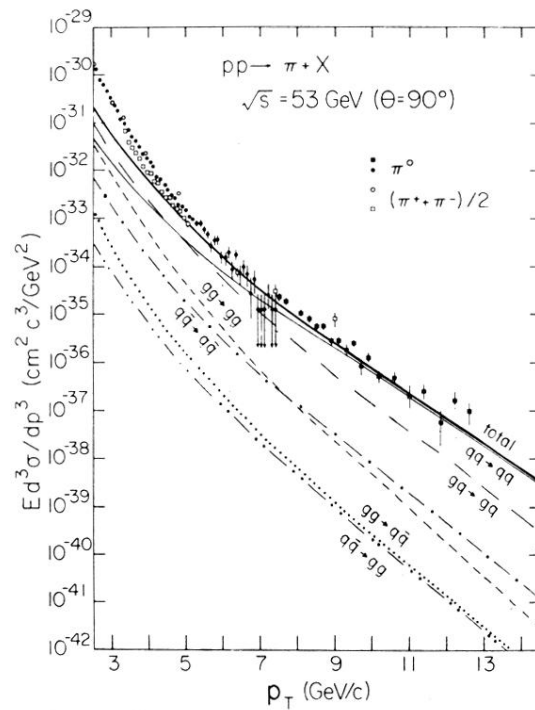


FIG. 6. Individual contributions of the various subprocesses to the solid curve of Fig. 4.

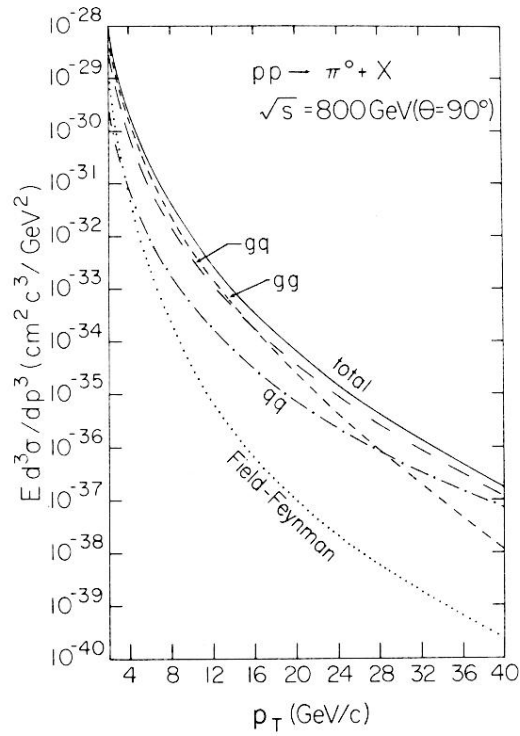


FIG. 7. Predictions for inclusive π^0 production using the Q^2 -dependent parton distributions of Ref. 9. The notation gg denotes the contribution from the sum of the $gg \rightarrow gg$ and $gg \rightarrow q\bar{q}$ subprocess, whereas gq stands for the sum of $gq \rightarrow gq$ and $g\bar{q} \rightarrow g\bar{q}$, and qq refers to the sum of $qq \rightarrow qq$, $q\bar{q} \rightarrow q\bar{q}$, $q\bar{q} \rightarrow gg$, and $\bar{q}q \rightarrow \bar{q}q$. The dotted curve shows the predictions of the model of Ref. 4.

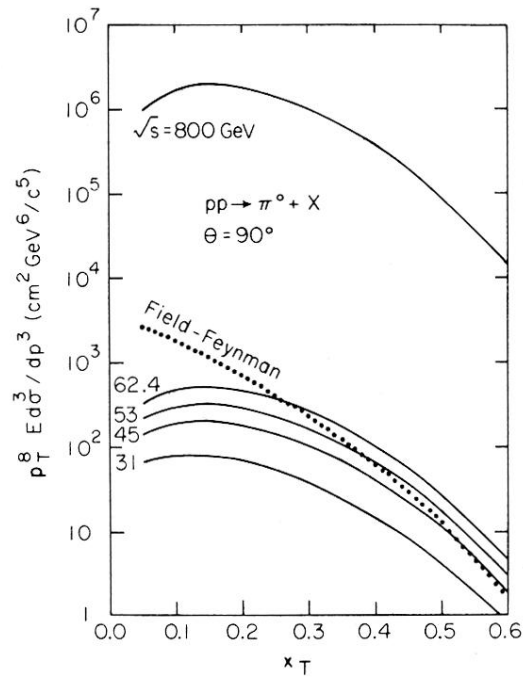


FIG. 8. Predictions for $p_T^8 E d^3 \sigma / dp^3$ for single- π^0 production at 90° . The parton distributions of Ref. 17 were used (see Ref. 42) and no Q^2 dependence was used in the fragmentation functions. The dotted curve shows the results of the model of Ref. 4.

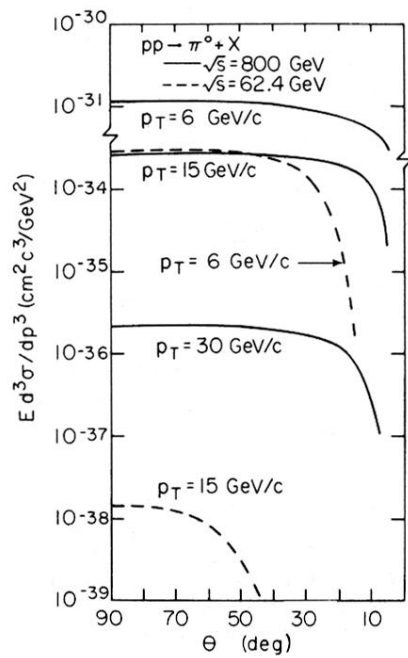


FIG. 9. Predictions for the angular dependence of the invariant cross section for $pp \rightarrow \pi^0 + X$ at several \sqrt{s} and p_T values. The parton distributions of Ref. 17 were used (see Ref. 42) and no Q^2 dependence was used in the fragmentation functions.